ACCOUNTS of chemical research

pubs.acs.org/accounts Article

Dynamic Electrodeposition on Bubbles: An Effective Strategy toward Porous Electrocatalysts for Green Hydrogen Cycling

Published as part of the Accounts of Chemical Research special issue "Electrosynthesis of Inorganic Materials".

Hui Jiang, Yujie Sun,* and Bo You*

Cite This: *Acc. Chem. Res.* 2023, 56, 1421−1432 Read Online

ACCESS | Metrics & More | Article Recommendations

CONSPECTUS: Closed-loop cycling of green hydrogen is a promising alternative to the current hydrocarbon economy for mitigating the energy crisis and environmental pollution. It stores energy from renewable energy sources like solar, wind, and hydropower into the chemical bond of dihydrogen (H_2) via (photo)electrochemical water splitting, and then the stored energy can be released on demand through the reverse reactions in H_2−O_2 fuel cells. The sluggish kinetics of the involved half-reactions like hydrogen evolution reaction (HER), oxygen evolution reaction (OER), hydrogen oxidation reaction (HOR), and oxygen reduction reaction (ORR) limit its realization. Moreover, considering the local gas−liquid−solid triphase microenvironments during H_2 generation and utilization, rapid mass transport and gas diffusion are critical as well. Accordingly, developing cost-effective and active electrocatalysts featuring three-dimensional hierarchically porous structures are highly desirable to promote the energy conversion efficiency. Traditionally, the synthetic approaches of porous materials include soft/hard templating, sol−gel, 3D printing, dealloying, and freeze-drying, which often need tedious procedures, high temperature, expensive equipment, and/or harsh physiochemical conditions. In contrast, dynamic electrodeposition on bubbles using the *in situ* formed bubbles as templates can be conducted at ambient conditions with an electrochemical workstation. Moreover, the whole preparation process can be finished within minutes/hours, and the resulting porous materials can be employed as catalytic electrodes directly, avoiding the use of polymeric binders like Nafion and the consequent issues like limited catalyst loading, reduced conductivity, and inhibited mass transport.

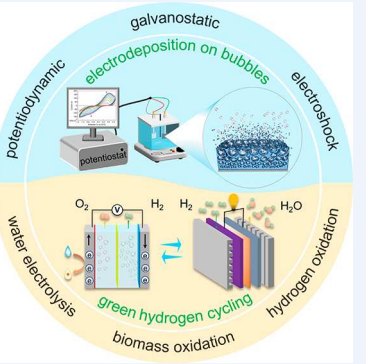

In this Account, we summarize our contributions to the dynamic electrodeposition on bubbles toward advanced porous electrocatalysts for green hydrogen cycling. These dynamic electrosynthesis strategies include potentiodynamic electrodeposition that linearly scans the applied potentials, galvanostatic electrodeposition that fixes the applied currents, and electroshock which quickly switches the applied potentials. The resulting porous electrocatalysts range from transition metals to alloys, nitrides, sulfides, phosphides, and their hybrids. We mainly focus on the 3D porosity design of the electrocatalysts by tuning the electrosynthesis parameters to tailor the behaviors of bubble co-generation and thus the reaction interface. Then, their electrocatalytic applications for HER, OER, overall water splitting (OWS), biomass oxidation (to replace OER), and HOR are introduced, with a special emphasis on the porosity-promoted activity. Finally, the remaining challenges and future perspective are also discussed. We hope this Account will encourage more efforts into this attractive research field of dynamic electrodeposition on bubbles for various energy catalytic reactions like carbon dioxide/monoxide reduction, nitrate reduction, methane oxidation, chlorine evolution, and others.

KEY REFERENCES

- Jiang, N.; You, B.; Sheng, M.; Sun, Y. Electrodeposited Cobalt-Phosphorous-Derived Films as Competent Bifunctional Catalysts for Overall Water Splitting. *Angew. Chem., Int. Ed.* **2015**, *54*, 6251−6254.[1] *This paper reports the potentiodynamic electrodeposition of porous bifunctional Co−P films for both HER and OER.*
- You, B.; Liu, X.; Hu, G.; Gul, S.; Yano, J.; Jiang, D. E.; Sun, Y. Universal Surface Engineering of Transition Metals for Superior Electrocatalytic Hydrogen Evolution in Neutral Water. *J. Am. Chem. Soc.* **2017**, *139*, 12283−12290.[2] *This paper describes the galvanostatic electrodeposition of a 3D hierarchically porous N−Ni framework for both neutral and alkaline HER.*
- Zhao, H.; Lu, D.; Wang, J.; Tu, W.; Wu, D.; Koh, S. W.; Gao, P.; Xu, Z. J.; Deng, S.; Zhou, Y.; You, B.; Li, H. Raw Biomass Electroreforming Coupled to Green Hydrogen

Received: January 31, 2023
Published: May 25, 2023

https://doi.org/10.1021/acs.accounts.3c00059
Acc. Chem. Res. 2023, 56, 1421−1432

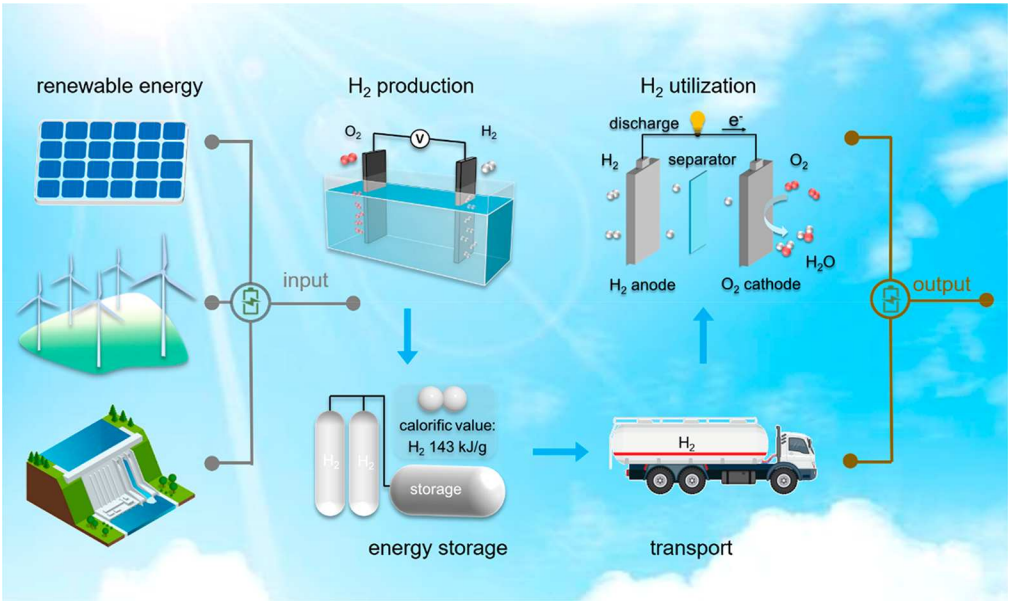

Figure 1. A simplified diagram of green hydrogen cycling.

Table 1. Comparison of Various Strategies toward Porous Materials Including Template, Pore Size, Advantages, and Disadvantages

method	template	pore size	advantages	disadvantages
soft templating	surfactants	micro/meso	controllable, high porosity	expensive, multistep, post-treatment
hard templating	porous solids	micro/meso/macro	controllable, versatile, high porosity	multistep, time-consuming, harsh leaching
sol−gel	template-free	micro	scalable, efficient	limited versatility, time-consuming, post-treatment
3D printing	template-free	macro	controllable, flexible	high cost, limited versatility, low porosity
dealloying	template-free	meso/macro	controllable	multistep, limited versatility, harsh leaching
freeze-drying	ices	meso/macro	ecofriendly, versatile	high cost, multistep, low porosity
electrodeposition on bubbles	*in situ* bubbles	meso/macro	rapid, versatile, scalable, ambient	moderate porosity

Generation. *Nat. Commun.* **2021**, *12*, 2008.[3] *This paper highlights the galvanostatic electrodeposition of a 3D hierarchically porous Ni framework for biomass oxidation upgrading.*

- Du, L.; Xiong, H.; Lu, H.; Yang, L.-M.; Liao, R.-Z.; Xia, B. Y.; You, B. Electroshock Synthesis of a Bifunctional Nonprecious Multi-Element Alloy for Alkaline Hydrogen Oxidation and Evolution. *Exploration* **2022**, *2*, 20220024.[4] *This paper elucidates the electroshock synthesis of 3D hierarchically porous NiCoCuMoW alloy for both HER and HOR.*

1. INTRODUCTION

The energy crisis and environmental pollution due to excessive depletion of nonrenewable fossil fuels accelerate the exploration of sustainable energy sources.[5,6] In response, a new energy paradigm based on green hydrogen cycling has been proposed as a promising alternative to the current fossil fuel-based hydrocarbon economy.[7] As shown in Figure 1, renewable energy resources, such as solar, wind, and hydropower, can be harvested to drive water splitting to produce H_2, which can be further stored and used as an energy carrier to release electric energy via H_2−O_2 fuel cells with no greenhouse gas emission.[8,9] The generation and utilization of H_2 involve four half-reactions including hydrogen evolution reaction (HER), oxygen evolution reaction (OER), hydrogen oxidation reaction (HOR), and oxygen reduction reaction (ORR). Their sluggish kinetics usually result in low efficiency.[10] Moreover, considering their local gas−liquid−solid triple-phase microenvironments, the interfacial mass transport and gas diffusion are also critical. Accordingly, cost-effective and active electrocatalysts with excellent mass transfer are necessary. It is known that hierarchically porous architectures with interconnected porosity and large specific surface area are beneficial for mass transport and exposure of active sites, conferring great potential for electrocatalysis.[11]

Currently, various synthetic approaches have been explored toward hierarchically porous materials including soft/hard templating that uses surfactants or porous solids as porogens[12] and template-free methods like sol−gel,[13] 3D printing,[14] dealloying,[15] and freeze-drying (Table 1).[16] In particular, dynamic electrodeposition on bubbles that employs *in situ* formed bubbles in electrolytes as templates is rapid, efficient, and scalable to obtain hierarchically porous structures under ambient conditions. Additionally, the resulting porous materials can be directly employed as catalytic electrodes, avoiding the use of polymeric binders like Nafion and the concomitant issues including limited catalysts loading, reduced conductivity, and inhibited mass transport. Specifically, taking dynamic hydrogen bubble-templated electrodeposition as an example, metal deposition from the corresponding salt solution is accompanied by HER. At the early stage, the competitive HER induces the supersaturation of dissolved H_2 and thus heterogeneous nucleation of bubbles takes place on the electrode surface followed by rapid growth of H_2 bubbles (Figure 2a).[17,18] The

https://doi.org/10.1021/acs.accounts.3c00059
Acc. Chem. Res. 2023, 56, 1421−1432

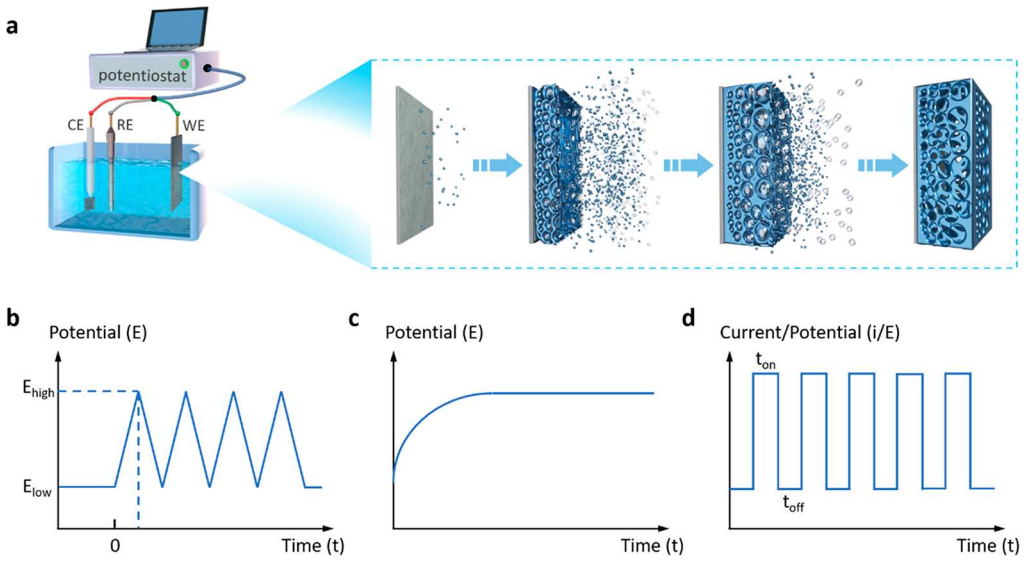

Figure 2. (a) Scheme of an electrodeposition device with the formation process of hierarchically porous materials by electrodeposition on bubbles. (b) Potential−time curve for potentiodynamic electrodeposition. (c) Recorded time-dependent potential in galvanostatic electrodeposition. (d) Pulsed signal applied in electroshock.

covering bubbles partially block the access of metal ions to the electrode and hence guide their electrodeposition around the electrode−bubble interface.[19] With the lapse of time, numerous bubbles could generate pores in the deposits with increasing thickness and walls, and the formed high-surface-energy sites on the electrode−bubble interface could in turn induce subsequent metal/bubble nucleation and deposition. Meanwhile, the coalescence of H_2 bubbles could disrupt the inward diffusion of metal ions, affecting metal deposition as well. It is expected that the pore size of deposits increases with the distance away from electrode surface due to the coalescence and growth of H_2 bubbles, leading to the formation of hierarchical porosity. Such a dynamic electrodeposition process was witnessed by Margaritondo's group in 2002 using phase-contrast radiology with synchrotron radiation.[20] These results imply that the parameters that can vary the behaviors of bubble and metal deposition including substrate features, applied potential/current, hydrodynamic conditions, and electrolyte additives, could modulate the porous structure of the resulting materials,[21] providing a powerful toolbox to interrogate the underlying porosity−activity correlation.

In this Account, we describe our recent progress in dynamic electrodeposition on bubbles to prepare advanced porous electrocatalysts to tackle the challenges in electrocatalytic green hydrogen cycling. Three innovative strategies including potentiodynamic electrodeposition, galvanostatic electrodeposition, and electroshock are presented. Subsequently, their electrocatalytic applications in HER, OER, overall water splitting (OWS), biomass oxidation (to replace OER), and HOR are discussed. The remaining challenges and future perspectives are presented finally.

2. DYNAMIC ELECTRODEPOSITION ON BUBBLES

Electrodeposition can be conducted under ambient conditions using an electrochemical workstation in a three (or two)-electrode configuration containing a working electrode (WE), a counter electrode (CE), and a reference electrode (RE) (or WE and CE), as shown in Figure 2a. Based on the manner of bubble generation, the dynamic electrodeposition can be divided into potentiodynamic electrodeposition, galvanostatic electrodeposition, and electroshock. Potentiodynamic electrodeposition means periodically and linearly scanning the potential between a high potential (E_{high}) and a low potential (E_{low}) (Figure 2b). Galvanostatic electrodeposition uses a fixed current, and the time-dependent potential response is recorded (Figure 2c).[22] Electroshock implies periodically switching the potential/current on and off (Figure 2d).

Considering the templating role of *in situ* electrogenerated bubbles, these different electrochemical modes would largely determine the bubble behavior, leading to various pore sizes and densities of the electrodeposited materials. Generally, potentiodynamic electrodeposition enables the periodical generation of bubbles and the oxidation/reduction of metal species at the triphase interface, beneficial to the growth of uniform and conformal porous materials. Galvanostatic electrodeposition generates bubbles continuously, which favors the nucleation, growth, coalescence, and fusion of bubbles, such that the as-prepared materials feature hierarchical porosity with large pore size and wide aperture distribution. Electroshock implies rapid generation and dissipation of bubbles, which inhibits in part the coalescence and fusion of bubbles and hence benefits the formation of relatively small and uniform pores. Moreover, other parameters that affect bubble behavior and metal species deposition, like substrate features (structure, type, and surface),[23] applied potentials/currents,[24] hydrodynamic conditions,[25] and electrolyte additives (surfactants, halides, and polymers),[26] could modulate the porous structures of the resulting materials as well.

2.1. Potentiodynamic Electrodeposition

Potentiodynamic electrodeposition is achieved via scanning potentials periodically within a certain potential window. The species on the electrolyte/electrode was repeatedly oxidized and reduced, beneficial to the growth of uniform and conformal porous films.[22] Our group used this method to successfully synthesize porous cobalt-sulfide films (Co−S) on fluorine-doped tin oxide (FTO) by consecutive linear scanning between −1.2 and 0.2 V vs Ag/AgCl.[27] Scanning electron microscopy (SEM) images revealed that both as-prepared and annealed

https://doi.org/10.1021/acs.accounts.3c00059
Acc. Chem. Res. 2023, 56, 1421−1432

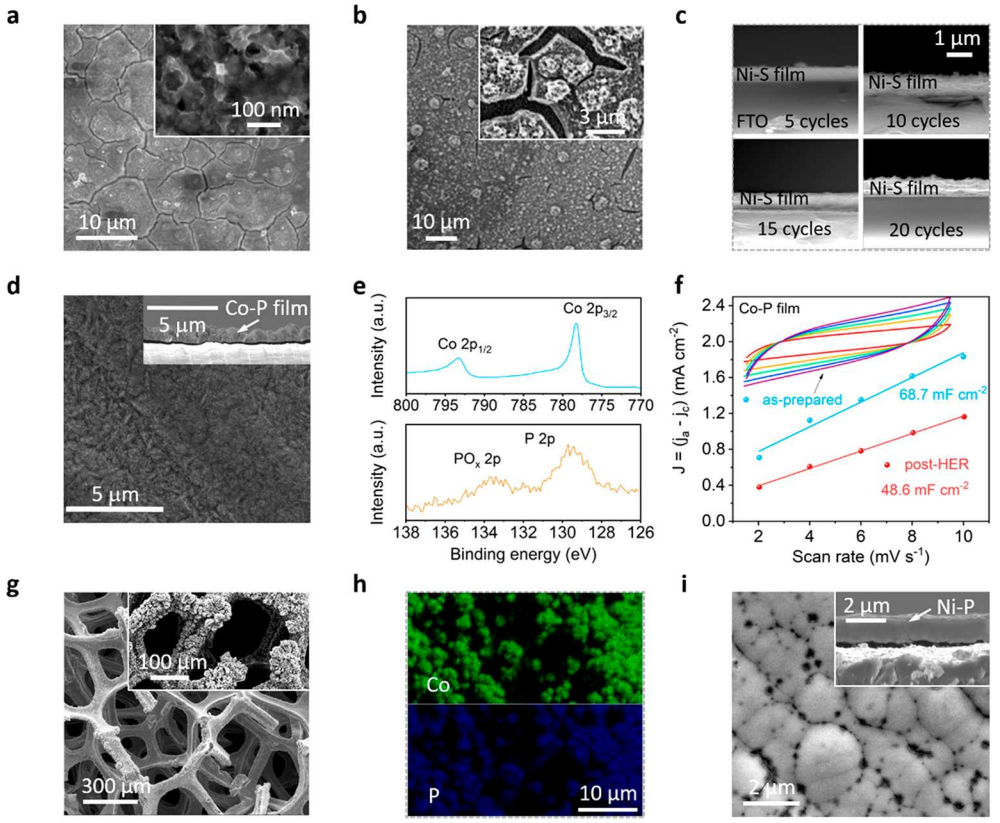

Figure 3. SEM images of (a) freshly prepared and (b) annealed Co−S. Reproduced with permission from ref 27. Copyright 2013 American Chemical Society. (c) Cross-section SEM images of Ni−S with different cycles. Reproduced with permission from ref 28. Copyright 2014 Royal Society of Chemistry. (d) SEM and cross-section images of fresh Co−P. (e) XPS spectra of Co−P. (f) Scan rate dependence of the current densities for Co−P before and after electrolysis. Reproduced with permission from ref 1. Copyright 2015 Wiley-VCH. (g) SEM and (h) elemental mapping images of Co−P/CF. Reproduced with permission from ref 29. Copyright 2016 American Chemical Society. (i) Top-view and cross-section SEM images of Ni−P. Reproduced with permission from ref 30. Copyright 2016 Wiley-VCH.

Co−S exhibited uniform porous morphology due to the evolution of H_2 bubbles during electrodeposition (Figure 3a,b). Such a facile potentiodynamic electrodeposition is also effective to synthesize porous amorphous nickel-sulfide films (Ni−S) with tunable thickness (Figure 3c).[28] Similarly, cobalt−phosphorus-derived films (Co−P) on Cu foil (CF) can be obtained as well.[1] SEM and cross-sectional SEM images (Figure 3d) revealed the complete coverage of Co−P with a thickness of 1−3 μm. X-ray photoelectron spectroscopy (XPS) revealed the metallic nature of Co and the phosphide-like form of P (Figure 3e). Electrochemically active surface areas (ECSAs) estimated from electrochemical double-layer capacitance (C_{dl}) unveiled that the Co−P before and after HER possessed much higher C_{dl} values (68.7 and 48.6 mF cm^{-2}) than a planar electrode (Figure 3f), suggesting their larger ECSAs. In addition, we also deposited Co−P on porous copper foam (Co−P/CF).[29] SEM and elemental mapping images (Figure 3g, h) suggested the uniform coverage of Co−P. The porous nickel−phosphorus film (Ni−P) can also be prepared by a similar method.[30] Due to the co-generation of H_2 bubbles, Ni−P showed black holes, as revealed by the SEM image (Figure 3i). The plentiful porosity is beneficial to mass transport and exposure of active sites.

2.2. Galvanostatic Electrodeposition

Galvanostatic electrodeposition refers to constant current electrolysis along with continuous bubble evolution as templates (Figure 2c), so that hierarchically porous architectures can be acquired. We used this strategy to prepare a hierarchically porous Ni framework on commercial Ni foam (hp-Ni) at −3.0 A cm^{-2} for 500 s.[31] The abundant macropores (~10 μm) were templated by H_2 bubbles (Figure 4a). As expected, the ECSA of hp-Ni was nearly 9 times higher than that of pristine nickel foam (NF) (Figure 4b). Besides monometallic porous materials, bimetallic frameworks can also be obtained via a similar galvanostatic electrodeposition. For example, by simply changing the Ni^{2+} precursor to a mixture of Ni^{2+} and Co^{2+} in the electrolyte, a bimetallic NiCo alloy framework could be obtained.[2] More recently, we synthesized porous pine needle-like Cu_3Ag_7 on copper foam (Cu_3Ag_7/CF) at −3.0 A cm^{-2} for only 30 s from an aqueous electrolyte containing both Ag^+ and Cu^{2+} species.[32] The high C_{dl} (51.8 mF cm^{-2}) relative to a planar electrode suggested larger ECSA and plentiful porosity of Cu_3Ag_7/CF.

In addition, we explored the synthesis of 3D hierarchically porous urchin-like Ni_2P superstructures on NF (Ni_2P/Ni/NF) via galvanostatic electrodeposition of hp-Ni followed by phosphorization.[33] SEM images (Figure 4c) of Ni_2P/Ni/NF indicated porous superstructures composed of stacked microspheres with urchin-like surface. Meanwhile, due to the formation of H_2 bubbles during electrodeposition, the macroporous walls of Ni_2P/Ni/NF featured numerous smaller macropores (~10 μm). The open primary and secondary macropores can facilitate substrate migration to the inner surface of Ni_2P/Ni/NF and favor outward diffusion of produced gases. Elemental mapping images (Figure 4d) revealed the uniform distribution of Ni and P in Ni_2P/Ni/NF. We also prepared

https://doi.org/10.1021/acs.accounts.3c00059
Acc. Chem. Res. 2023, 56, 1421−1432

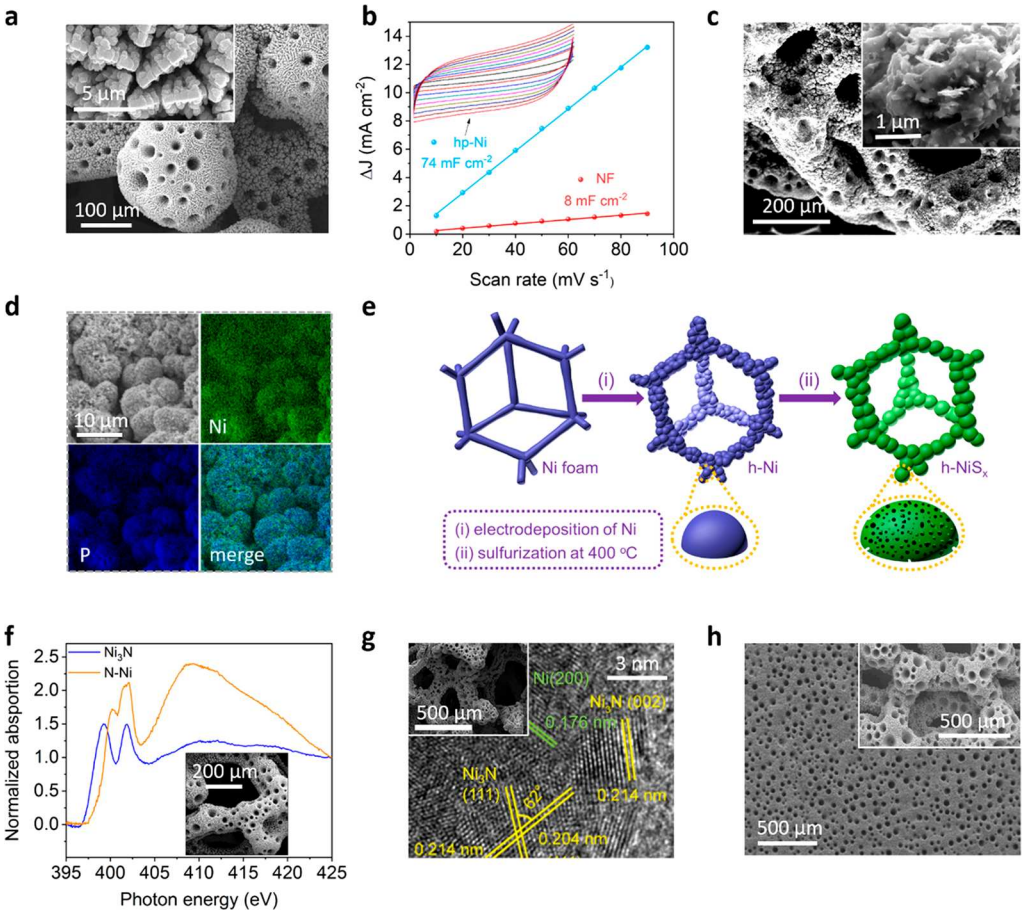

Figure 4. (a) SEM images of hp-Ni. (b) CV curves and scan rate dependence of the current densities of hp-Ni and NF. Reproduced with permission from ref 31. Copyright 2017 American Chemical Society. (c) SEM images and (d) elemental mapping of Ni_2P/Ni/NF. Reproduced with permission from ref 33. Copyright 2015 American Chemical Society. (e) Synthetic scheme for hp-NiS_x. Reproduced with permission from ref 34. Copyright 2016 Wiley-VCH. (f) N K-edge XANES spectra of N−Ni and Ni framework with the SEM image of N−Ni. Reproduced with permission from ref 2. Copyright 2017 American Chemical Society. (g) HR-TEM and SEM images of the Ni_3N/Ni interface. Reproduced with permission from ref 35 under the terms of a CC-BY 4.0 license. Copyright 2018 The Authors, published by Springer Nature. (h) SEM images of Co_2N/Ni/CP and Co_2N/Ni/CF (inset). Reproduced with permission from ref 36. Copyright 2019 American Chemical Society.

hierarchically porous nickel sulfide superstructures (h-NiS_x) with both macropores and mesopores via a similar galvanostatic electrodeposition followed by sulfurization (Figure 4e).[34]

Inspired by the high specific surface area of hp-Ni, we obtained diverse surface nitrogen modified porous metals (e.g., N−Ni, N−Fe, N−Co, N−Cu, and N−NiCo alloy) by galvanostatic electrodeposition and subsequent low-temperature ammonium carbonate treatment.[2] The SEM image (Figure 4f, inset) revealed an interconnected 3D macroporous network for N−Ni. The N K-edge XANES spectrum (Figure 4f) showed a positive shift to higher energy for N−Ni relative to Ni_3N, indicative of weaker interaction and less electron transfer from Ni to N in N−Ni.[2]

Furthermore, partially nitriding the hp-Ni through high-temperature annealing in ammonia creates the interfaces between Ni and Ni_3N in the resulting 3D macroporous Ni_3N/Ni/NF (Figure 4g, inset).[35] Their high-resolution transmission electron microscopy (HR-TEM) image clearly showed the interface of hexagonal Ni_3N and cubic Ni. A similar structure (Figure 4h) could be obtained via partial nitridation of cobalt nanoparticles on cobalt foam (Co_2N/Co/CF) or carbon paper (Co_2N/Co/CP).[36]

2.3. Electroshock

Electroshock that rapidly switches potentials or currents on and off enables quick bubble generation and dissipation and thus partially inhibits their coalescence and fusion, beneficial to the formation of relatively small and uniform porous structures.[37,38] We synthesized a porous NiCoCuMoW multielement alloy (MEA) by electroshock in which pulsed potential of −6 V was applied with an on time of 0.2 s and an off time of 0.8 s for 400 cycles (Figure 5a).[4] SEM images (Figure 5b) revealed an inherited 3D porosity of the NF skeleton covered by coarse stacked particles with numerous cavities. Elemental mapping images suggested the uniform distribution of Ni, Co, Cu, Mo, and W (Figure 5c). X-ray diffraction (XRD) (Figure 5d) analysis revealed a body-centered cubic structure (BCC) crystal for NiCoCuMoW, similar to reported results.[39]

3. POROUS ELECTROCATALYSTS FOR GREEN HYDROGEN CYCLING

3.1. Hydrogen Evolution

As a vital half-reaction in water splitting, HER is of great significance for green hydrogen cycling.[40] In view of the multistep pathway, an ideal HER electrocatalyst should have optimal affinity/repellency to balance the sorption/diffusion of

https://doi.org/10.1021/acs.accounts.3c00059
Acc. Chem. Res. 2023, 56, 1421−1432

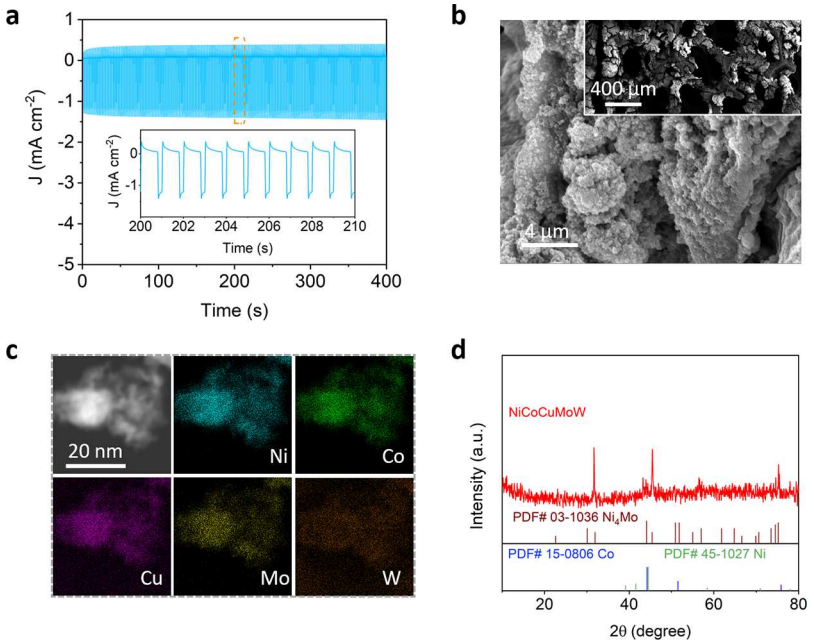

Figure 5. (a) Current density−time curve in electroshock electrodeposition. (b) SEM images, (c) elemental mapping, and (d) XRD pattern of the NiCoCuMoW MEA. Reproduced with permission from ref 4. Copyright 2022 Wiley-VCH.

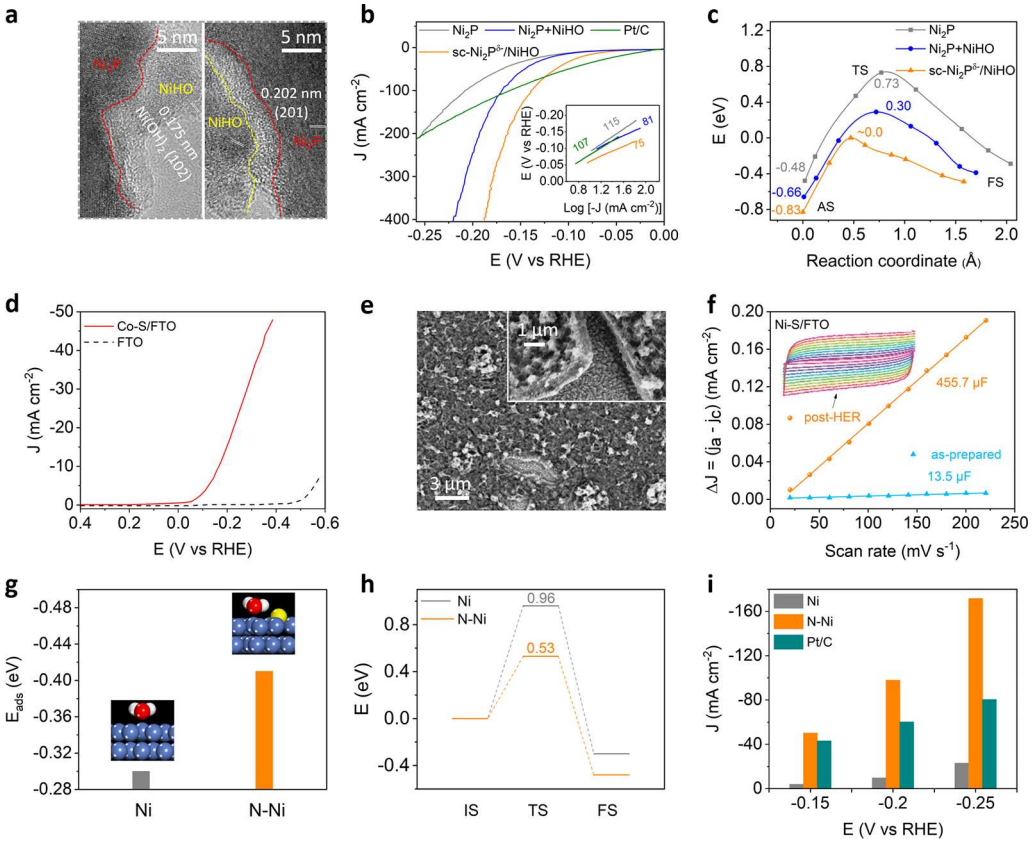

Figure 6. (a) HR-TEM images of sc-$Ni_2P^{\delta-}$/NiHO (left) and Ni_2P + NiHO control (right). (b) LSV curves for sc-$Ni_2P^{\delta-}$/NiHO and controls, along with the corresponding Tafel slopes. (c) Reaction energy diagrams of the elemental steps in alkaline HER on $Ni_2P(111)$, $Ni_2P(111)$ + NiHO and sc-$Ni_2P^{\delta-}(111)$/NiHO. Reproduced with permission from ref 43. Copyright 2019 Wiley-VCH. (d) Polarization curves of annealed Co−S after 3 h electrolysis and FTO substrate. (e) SEM images of Co−S after 3 h electrolysis. Reproduced with permission from ref 27. Copyright 2013 American Chemical Society. (f) Scan rate dependence of current densities and the CV curves (inset) of Ni−S. Reproduced with permission from ref 28. Copyright 2014 Royal Society of Chemistry. (g) Adsorption energy of water and (h) free energy barrier profiles of water dissociation on Ni(111) and N−Ni(111). (i) Comparison of current densities at different overpotentials for N−Ni, Ni framework, and Pt/C for neutral HER. Reproduced with permission from ref 2. Copyright 2017 American Chemical Society.

https://doi.org/10.1021/acs.accounts.3c00059
Acc. Chem. Res. 2023, 56, 1421−1432

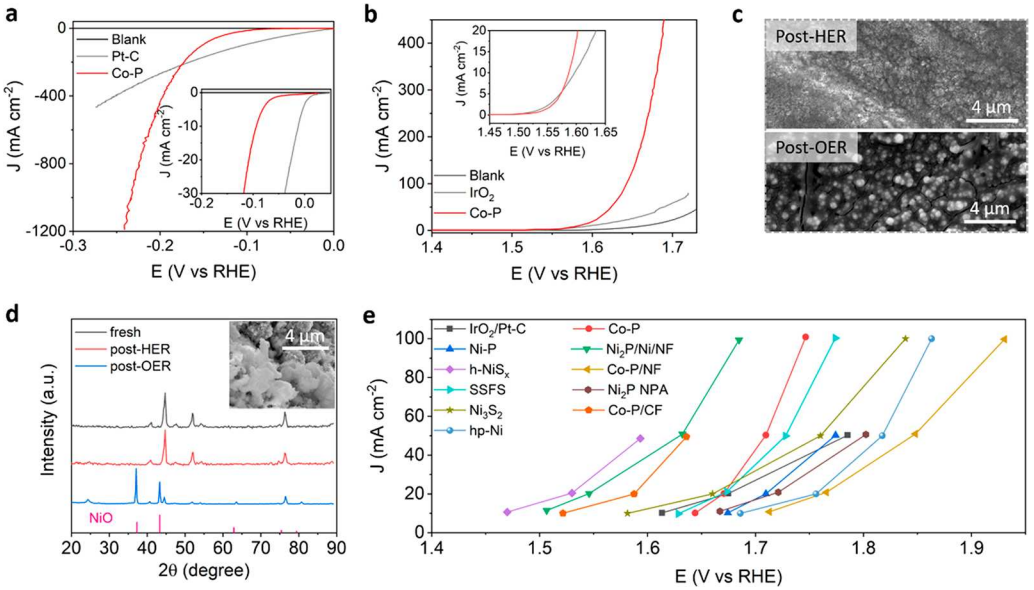

Figure 7. LSV curves for (a) HER and (b) OER over Co−P. (c) SEM images of post-HER and post-OER Co−P. Reproduced with permission from ref 1. Copyright 2015 Wiley-VCH. (d) XRD pattern for fresh, post-HER, and post-OER Ni_2P/Ni/NF samples with the SEM image of post-OER Ni_2P/Ni/NF. Reproduced with permission from ref 33. Copyright 2015 American Chemical Society. (e) Comparison of overall water splitting performance for our reported bifunctional electrocatalysts.

intermediates/substrates, which are mainly governed by the surface charge density and porosity of the electrocatalyst.[41,42] We therefore fabricated strong electronically coupled and negatively charged porous nickel phosphide/nickel hydr(oxy)-oxides hybrids (sc-$NiP_2^{\delta-}$/NiHO) via galvanostatic electrodeposition followed by phosphorization and *in situ* electrochemical oxidation.[43] As shown in Figure 6a, the interplanar spacing of NiHO in sc-$Ni_2P^{\delta-}$/NiHO was calculated to be 0.175 nm, suggesting the successful partial oxidation of Ni_2P to $Ni(OH)_2$. The tight contact between Ni_2P and NiHO in sc-$Ni_2P^{\delta-}$/NiHO (Figure 6a), different from the gaps in the Ni_2P + NiHO control, revealed their strong electronic coupling.[43] Linear sweep voltammetry (LSV) was then conducted to investigate their HER performance in 1.0 M KOH (Figure 6b). The overpotential at 10 mA cm^{-2} (η_{10}) for sc-$Ni_2P^{\delta-}$/NiHO was only 60 mV, lower than those of fresh Ni_2P (90 mV) and Ni_2P + NiHO (85 mV). The smaller Tafel slope further underscored more favorable HER kinetics on sc-$Ni_2P^{\delta-}$/NiHO (Figure 6b, inset). DFT calculations suggested that the negatively charged Ni_2P surface in sc-$Ni_2P^{\delta-}$/NiHO favor the adsorption of electron-deficient H atom in H_2O and facilitate subsequent water dissociation by repelling the electron-rich OH in H_2O. As presented in Figure 6c, the adsorption energy (−0.83 eV) for the H_2O adsorption state (AS) and the energy barrier (0.83 eV) for the transition state (TS) of water dissociation on sc-$Ni_2P^{\delta-}$/NiHO were significantly lower than those on fresh Ni_2P (−0.48 and 1.21 eV) and Ni_2P + NiHO (−0.66 and 0.96 eV).

In addition, interfacing porous Ni and Ni_3N can also optimize water and hydrogen adsorption. The best hydrogen adsorption site on porous Ni_3N/Ni/NF exhibited a H adsorption energy (ΔG_{H^*}) of 0.01 eV, very close to the ideal amount of 0 eV.[35] Ni_3N/Ni/NF demonstrated excellent HER activity with η_{10} of only 12 mV in 1.0 M KOH. Even in a neutral potassium phosphate (KPi) buffer, the η_{10} of Ni_3N/Ni/NF was low at 19 mV. We then extended this interfacing strategy to prepare porous Co-based electrocatalysts on cobalt foam (Co_2N/Co/CF) or carbon paper (Co_2N/Co/CP).[36] Remarkably, the η_{10} of Co_2N/Co/CF was only 12 mV.

Given the corrosiveness and environmental issues caused by the use of strong acidic and alkaline electrolytes, we developed advanced catalysts for neutral HER. For example, we prepared a porous Co−S via potentiodynamic electrodeposition on FTO for HER in neutral 1.0 M KPi.[27] After electrolysis activation, the η_{50} was lowered to 397 mV (Figure 6d). Elemental analysis of the Co−S after 3 h electrolysis showed the retention of Co−S, consistent with SEM characterizations (Figure 6e). Analogous activation during neutral HER was observed for the porous Ni−S,[28] as indicated by the increased C_{dl} from 13.5 to 455.7 μF after electrolysis (Figure 6f). We speculated that the activation process is caused by evolved H_2 bubbles, which induce surface reorganization of the underlying electrocatalysts.

Recently, we found that surface nitrogen modification can considerably enhance the activity of first-row transition metal frameworks for neutral HER (Figure 6g−i).[2] Using the porous Ni framework as an example, DFT calculations showed that the electron-rich nitrogen in N−Ni facilitates water adsorption via the electron-deficient H atom as revealed by the enhanced adsorption energy (E_{ads}) from −0.30 eV to −0.41 eV (Figure 6g). Also, the energy barrier for water dissociation on N−Ni was decreased from 0.96 to 0.53 eV (Figure 6h), indicative of promoted water dissociation. Consequently, the resulting N−Ni rivaled Pt/C for HER at pH 7 (Figure 6i).

3.2. Overall Water Splitting

The efficiency of water splitting is mainly limited by OER. To simplify electrolyzer configuration, we explored porous bifunctional electrocatalysts with both OER and HER activities in the same electrolyte to achieve overall water splitting. For instance, the electrocatalytic HER, OER, and OWS performance of Co−P were investigated in 1.0 M KOH.[1] As shown in Figure 7a, the η_{10} of Co−P for HER was only 94 mV (Figure 7b). After 24 h electrolysis of HER, the post-HER Co−P still maintained a uniform coverage and morphology (Figure 7c). Regarding OER, subsequently, the η_{10} of Co−P was 345 mV, smaller than that of

https://doi.org/10.1021/acs.accounts.3c00059
Acc. Chem. Res. 2023, 56, 1421−1432

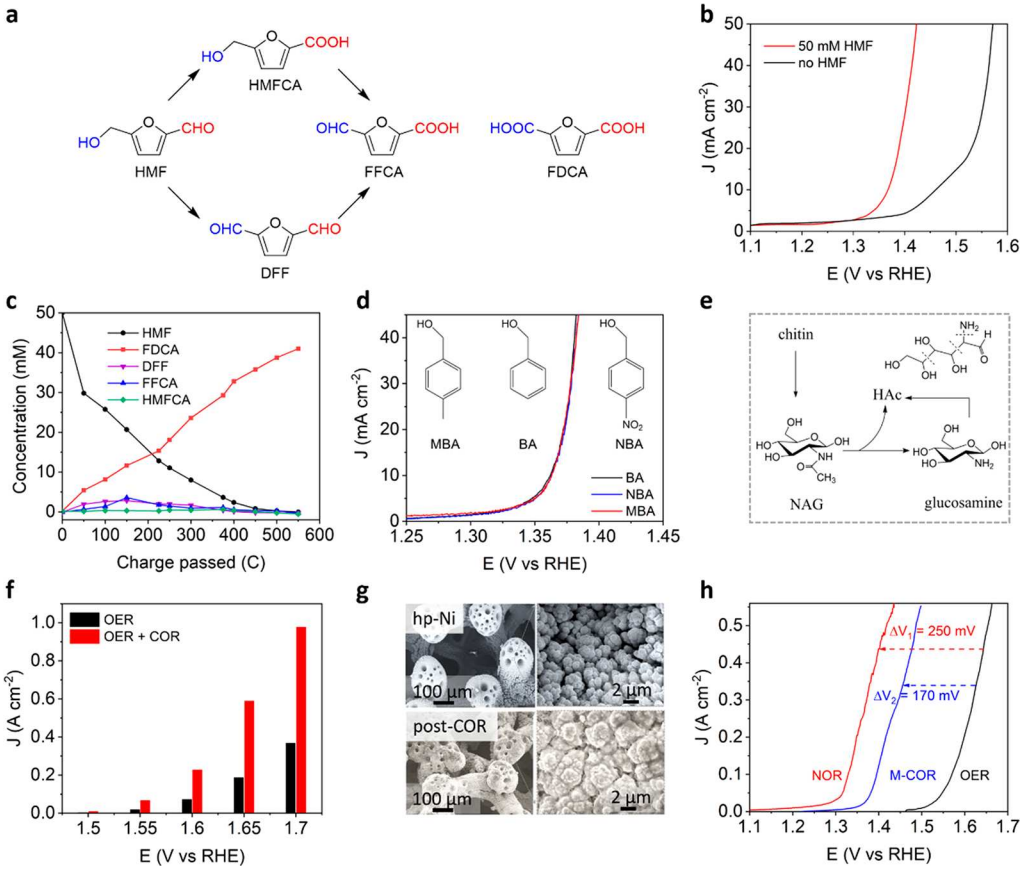

Figure 8. (a) Two possible pathways of HMF oxidation to FDCA. (b) LSV curves of Co−P/CF in 1 M KOH with and without 50 mM HMF. (c) Conversion of HMF and yields of oxidation products over passed charge during electrolysis at 1.423 V vs RHE in 1.0 M KOH containing 50 mM HMF. Reproduced with permission from ref 29. Copyright 2016 American Chemical Society. (d) LSV curves on hp-Ni in 1.0 M KOH with 10 mM MBA, BA, and NBA, together with their corresponding chemical structures. Reproduced with permission from ref 31. Copyright 2017 American Chemical Society. (e) Possible main reaction pathways of chitin oxidation. (f) Comparison of current densities at various potentials in 1.0 M KOH with and without 33.3 mg L^{-1} chitin. (g) SEM images of fresh and post-COR hp-Ni. (h) LSV curves of anodic reactions in 1.0 M KOH containing 2.2 g L^{-1} NAG or 3.5 g L^{-1} milled chitin, and OER. Reproduced from ref 3 under the terms of the CC-BY 4.0 license. Copyright 2021 The Authors, published by Springer Nature.

IrO_2 (Figure 7b). Interestingly, the post-OER Co−P showed large nanoparticle aggregates (Figure 7c), suggesting *in situ* surface reconstruction to OER-active cobalt oxides/(oxy)-hydroxides.[1] For OWS in 1.0 M KOH, the Co−P couple exhibited larger current density than that of IrO_2/Pt−C at 1.67 V. Likewise, the porous Ni−P also displayed bifunctional HER and OER performance.[30]

To further accelerate the electrocatalytic kinetics, we synthesized 3D hierarchical and interconnected macroporous Ni_2P/Ni/NF.[33] For HER, its current density beyond −112 mV also largely exceeded that of Pt/C. A 20 h HER stability test did not alter the composition and urchin-like morphology of Ni_2P/Ni/NF (Figure 7d). Additionally, Ni_2P/Ni/NF exhibited excellent OER activity with a small η_{10} of 200 mV. SEM images (Figure 7d, inset) of the post-OER Ni_2P/Ni/NF revealed the featureless monoliths plus urchin-like microparticles, different from that for fresh Ni_2P/Ni/NF (Figure 4c), suggesting a similar *in situ* surface oxidation reconstruction. A Ni_2P/Ni/NF couple-based alkaline water electrolyzer reached 10 and 100 mA cm^{-2} at cell voltages of 1.49 and 1.68 V, respectively. The improved activity of Ni_2P/Ni/NF originated from its 3D interconnected porosity and high ECSA.[33] In addition, the bifunctional catalytic activity of hierarchically porous h-NiS_x was also explored.[34] As shown in Figure 7e, the h-NiS_x couple required a voltage of only 1.47 V to afford 10 mA cm^{-2} for OWS in 1.0 M KOH. The alkaline OWS performance for other bifunctional electrocatalysts reported by us was also included in Figure 7e.[1,29−31,33,34,44−47]

3.3. Biomass Oxidation

Although developing active electrocatalysts can reduce the overpotential of OER for efficient water splitting to generate H_2, this reduction is insufficient. Moreover, the low value of O_2, possible crossover of H_2/O_2, and detrimental effects of reactive oxygen species (ROS) may pose cost and safety issues.[47,48] We therefore reason that replacing OER with more favorable organic oxidation reactions is economically attractive. This strategy can not only circumvent H_2/O_2 mixing and ROS formation, but also reduce the voltage input for H_2 production, as well as generate value-added products at the anode. Among biomass-derived intermediates, 5-hydroxymethylfurfural (HMF) is a platform precursor (Figure 8a). For instance, 2,5-furandicarboxylic acid (FDCA), one of the valuable oxidation products of HMF, has been regarded as a green replacement of terephthalic acid to synthesize polyamides, polyesters, and polyurethanes.[47]

Interestingly, the porous Co−P can be directly utilized to catalyze HMF oxidation to FDCA in 1.0 M KOH.[29] For example, the Co−P on copper foam (Co−P/CF) achieved 20

https://doi.org/10.1021/acs.accounts.3c00059
Acc. Chem. Res. 2023, 56, 1421−1432

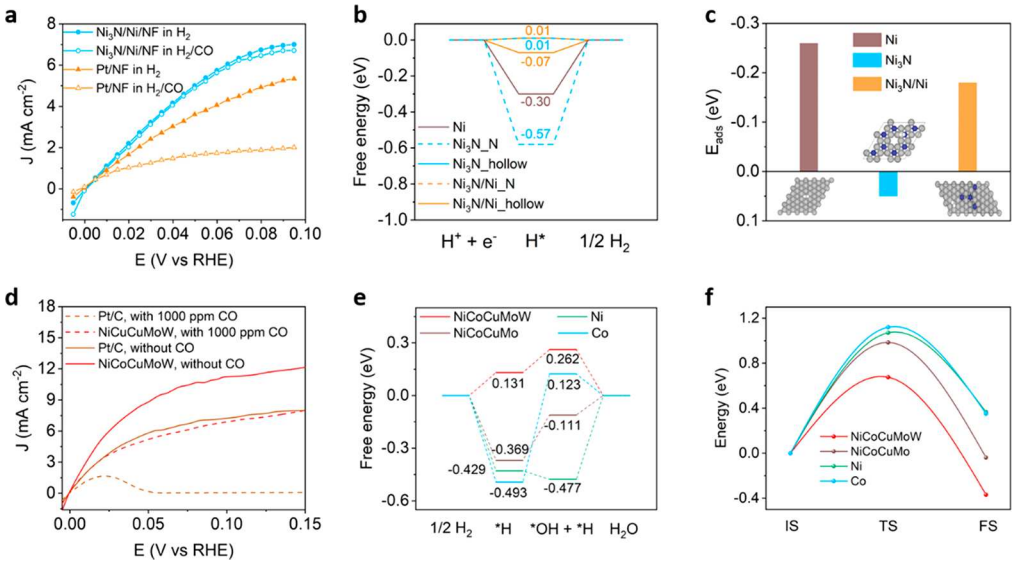

Figure 9. (a) Comparison of HOR polarization curves of Ni_3N/Ni/NF and Pt/NF in 0.1 M KOH saturated with H_2 or H_2 with 2% CO (v/v). (b) Hydrogen adsorption free energy, (c) adsorption energy of H_2 on Ni, Ni_3N, and Ni_3N/Ni. Reproduced from ref 35 under the terms of the CC-BY 4.0 license. Copyright 2018 The Authors, published by Springer Nature. (d) Comparison of the polarization curves and Tafel plots of NiCoCuMoW and Pt/C in 1.0 M KOH saturated with H_2 or H_2 with 1000 ppm of CO. (e) Gibbs free-energy and (f) reaction energy barrier diagrams of alkaline HOR pathway on Ni, Co, NiCoCuMo, and NiCoCuMoW. Reproduced with permission from ref 4. Copyright 2022 Wiley-VCH.

mA cm^{-2} at 1.38 V vs RHE with 50 mM HMF, which was smaller than that for OER (1.53 V vs RHE, Figure 8b). Product quantification (Figure 8c) confirmed a nearly 90% yield of FDCA. Subsequently, a two-electrode electrolyzer based on Co−P/CF for simultaneous production of FDCA and H_2 was constructed, and the electrocatalyst couple required only 1.44 V to achieve 20 mA cm^{-2}, whereas a higher voltage of 1.59 V was required for OWS.

Encouraged by the above results, we continued to explore the oxidative upgrading of various alcohols paired with H_2 co-production.[47] To avoid the potential influence of nonmetal elements in the catalyst composition, we purposely prepared a 3D hierarchically porous hp-Ni.[31] Benzyl alcohol (BA), 4-nitrobenzyl alcohol (NBA), and 4-methylbenzyl alcohol (MBA) (Figure 8d) were selected as the organic substrates. Surprisingly, we found that the electronic effects of diverse substituents at the para position of BA have negligible impact on their electro-oxidation over hp-Ni, as indicated by the overlapped LSV curves (Figure 8d). We speculated that oxidation of these three alcohols primarily depended on the potential to realize a high oxidation state of nickel species, instead of the intrinsic thermodynamics. Recently, we extended the organic substrates to raw biomass, chitin, the most abundant natural amino biopolymer found in nature.[3] Figure 8e shows its possible main reaction pathways. The monomer of chitin, *N*-acetylglucosamine (NAG), can be oxidized to acetic acid (HAc) and glucosamine by deacetylation, which can be further converted to HAc by opening the pyranose ring. As plotted in Figure 8f, the current density for chitin oxidation reaction (COR) was larger than that of OER at the same potential. The morphology retention (Figure 8g) of the hp-Ni after 4 h of COR electrolysis suggested its long-term stability. Milling chitin (M-chitin) can increase its solubility to 3.5 g L^{-1}, and the LSV curve (Figure 8h) for milled-chitin oxidation reaction (M-COR) showed much higher current density with a decreased potential by ∼170 mV compared to OER under the investigated current densities. This oxidation potential can be further reduced by ∼250 mV using the monomer of chitin, NAG, as a substrate (NAG oxidation reaction, NOR).

3.4. Hydrogen Oxidation

Apart from efficient H_2 generation from water splitting, the utilization of H_2 via H_2−O_2 fuel cells to produce electricity on demand is equally important, such that advanced electrocatalysts are needed to accelerate the kinetics of involved H_2 oxidation reaction (HOR).[49] Accordingly, we explored the porous interface of Ni and Ni_3N.[35] The HOR performance of Ni_3N/Ni/NF was investigated in H_2-saturated 0.1 M KOH. Compared to Pt/NF, Ni_3N/Ni/NF exhibited more superior HOR activity (6.95 vs 5.25 mA cm^{-2} at 0.09 V vs RHE, Figure 9a) and higher tolerance against CO poisoning. DFT computations suggested that the ΔG_{H^*} of two interfacial sites (Ni_3N/Ni_N and Ni_3N/Ni_hollow) were close to the ideal value of 0 eV (0.01 and −0.07 eV), higher than that of pure Ni (−0.30 eV) (Figure 9b). As for Ni_3N, there existed one type of site which had a ΔG_{H^*} of 0.01 eV but also another type of site exhibiting very strong hydrogen affinity with calculated ΔG_{H^*} close to −0.57 eV. Furthermore, the Ni_3N/Ni interface and Ni possessed stronger H_2 adsorption than Ni_3N, indicating favored H_2 adsorption on Ni_3N/Ni and Ni (Figure 9c). Both the ideal ΔG_{H^*} (0.01 and −0.07 eV, Figure 9b) and strong H_2 adsorption (Figure 9c) of Ni_3N/Ni supported its excellent HOR performance. Similarly, the interfacial sites of Co_2N/Co/NF also exhibited improved HOR performance.[36]

Recently, our group reported an electroshock method toward a rous NiCoCuMoW MEA for alkaline HOR and HER.[4] The NiCoCuMoW afforded 11.2 mA cm^{-2} at 0.1 V vs RHE for HOR, higher than those for NiCoCuMo (7.1 mA cm^{-2}) and Pt/C (Figure 9d). Benefiting from the multi-active-site nature, CO poisoned NiCoCuMoW was still comparable to Pt/C under pure H_2 feeding. In contrast, Pt/C suffered from severe CO poisoning and lost its activity completely at potentials exceeding 0.05 V vs RHE. Note that hydrogen binding energy (HBE) and/or hydroxide binding energy (OHBE) are critical for alkaline HOR. Figure 9e shows that Co(111) and NiCoCuMo(111)

https://doi.org/10.1021/acs.accounts.3c00059
Acc. Chem. Res. 2023, 56, 1421−1432

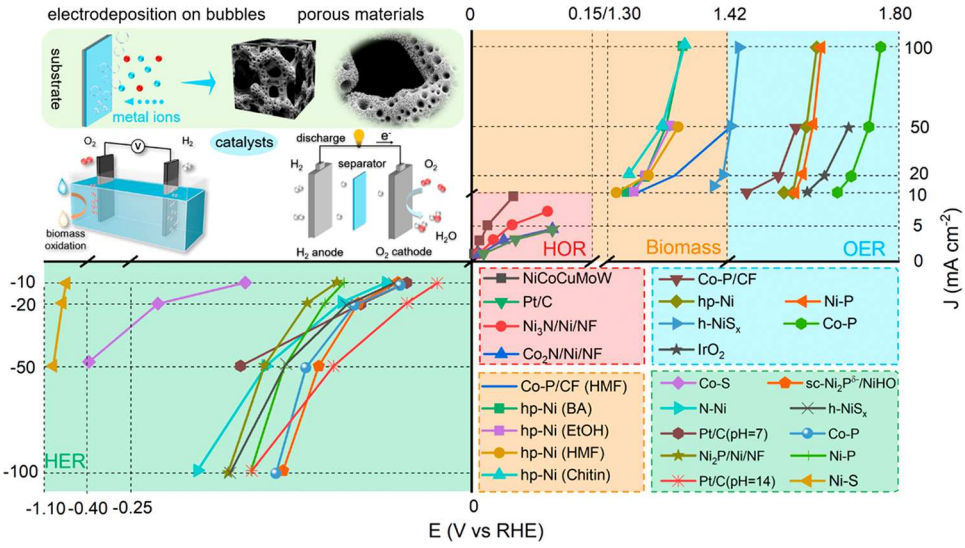

Figure 10. Summary of diverse electrocatalysts prepared by dynamic electrodeposition on bubbles for various reactions in green hydrogen cycling.

possess too strong H binding and too weak OH binding, accounting for their poor HOR activity. Although Ni(111) revealed an appropriate OHBE (−0.018 eV), the strong H binding (−0.429 eV) led to a high energy barrier (0.477 eV) for the combination of *H and *OH to H_2O. In contrast, NiCoCuMoW(111) exhibited similar HBE and OHBE of 0.131 eV. Kinetic analysis confirmed the low energy barrier of NiCoCuMoW for HOR (0.675 eV) relative to control samples (Figure 9f). These thermodynamic and kinetic results clearly indicated the great HOR activity of NiCoCuMoW MEA.

4. SUMMARY AND OUTLOOK

This Account has summarized our recent work of dynamic electrodeposition on bubbles toward advanced porous electrocatalysts for green hydrogen generation from water splitting and utilization in H_2−O_2 fuel cells. These electrosynthesis methodologies include potentiodynamic, galvanostatic, and electroshock electrodepositions and the resulting porous electrocatalysts range from metals to alloys, nitrides, sulfides, phosphides, and their hybrids, with promising performance for HER, OWS, biomass oxidation, and HOR (Figure 10). Looking ahead, there are still some challenges that deserve further investigation.

First, assisted by advanced electrochemistry and microscopic characterizations, we have preliminarily determined the nucleation, growth, and template role of bubbles,[50] while full understanding of the whole electrodeposition is still not yet complete due to the complex convolution of reaction, transport, and interface which involve multiple processes like bubble formation, mass transport, and species deposition at the triphase interface, and the dynamic changes of surface forces, lubrication, intermolecular force, electric field, adsorption, and so on. Therefore, more advanced operando techniques along with their combination are desirable to provide multidimensional information on the dynamic interface. How to accurately control the bubble formation, size, and density, and identify the underlying origins necessitates long-term research. In fact, recent works of mesostructure-induced selectivity in CO_2 reduction reported by Surendranath's group imply that the assumption of high porosity benefiting the exposure of active sites and mass transport may be too simplistic.[51,52] Instead, deep understanding of the complex interplay at electrocatalytic interface deserves further study.

Second, although the dynamic electrodeposition on bubbles is simple, rapid, and environmentally benign, it commonly obtains porous electrocatalysts on a small conductive substrate in the laboratory. The scaling-up for membrane electrode assemblies may suffer from severe controllability issues due to abundant bubble aggregation and evolution. Massive bubbles like H_2 may pose safety issues as well. Therefore, novel devices and protocols for scalable electrosynthesis are needed for practical applications. Alternatively, exploring the *in situ* electrochemical generation of inert or nonexplosive gases like N_2 and CO_2 for templating could be appealing options, awaiting further investigation.

Third, closing the green hydrogen cycling needs advanced electrocatalysts for the oxygen reduction reaction (ORR), a cathode half-reaction in H_2−O_2 fuel cells. In fact, ORR is thermodynamically more challenging than HOR. Its kinetics, even on Pt benchmarks, is still sluggish.[53,54] It is thus worth exploring the synthesis of porous ORR electrocatalysts by dynamic electrodeposition on bubbles. However, to our knowledge, relevant works have been rarely reported.

AUTHOR INFORMATION

Corresponding Authors

Yujie Sun − *Department of Chemistry, University of Cincinnati, Cincinnati, Ohio 45221, USA;* orcid.org/0000-0002-4122-6255; Email: yujie.sun@uc.edu

Bo You − *Key Laboratory of Material Chemistry for Energy Conversion and Storage, Ministry of Education, Hubei Key Laboratory of Material Chemistry, and Service Failure, School of Chemistry and Chemical Engineering, Huazhong University of Science and Technology, Wuhan, Hubei 430074, China;* orcid.org/0000-0003-1849-0418; Email: youbo@hust.edu.cn

Author

Hui Jiang − *Key Laboratory of Material Chemistry for Energy Conversion and Storage, Ministry of Education, Hubei Key Laboratory of Material Chemistry, and Service Failure, School*

https://doi.org/10.1021/acs.accounts.3c00059
Acc. Chem. Res. 2023, 56, 1421−1432

of Chemistry and Chemical Engineering, Huazhong University of Science and Technology, Wuhan, Hubei 430074, China

Complete contact information is available at:
https://pubs.acs.org/10.1021/acs.accounts.3c00059

Author Contributions

CRediT: **Hui Jiang** writing-original draft (equal); **Yujie Sun** writing-review & editing (supporting); **Bo You** conceptualization (lead), funding acquisition (lead), project administration (lead), supervision (lead), writing-original draft (equal), writing-review & editing (lead).

Notes

The authors declare no competing financial interest.

Biographies

Hui Jiang is a Ph.D. candidate at Huazhong University of Science and Technology. His research interests include the synthesis of inorganic nanomaterials for energy catalysis.

Yujie Sun obtained his Ph.D. degree in 2010 under the supervision of Prof. Claudia Turro at The Ohio State University. Subsequently, he joined Prof. Christopher J. Chang's group at the University of California, Berkeley, and Lawrence Berkeley National Laboratory as a postdoctoral scholar. Yujie started his independent career at Utah State University in 2013, moved to the University of Cincinnati in 2018, and was promoted to professor in 2023. His group is interested in developing and understanding novel materials and molecules for catalysis and biomedical applications.

Bo You received his Ph.D. degree in 2014 under the supervision of Prof. Zhaoxiang Deng at University of Science and Technology of China. He then joined Prof. Yujie Sun's group at Utah State University, Prof. Hong Li's group at Nanyang Technological University, and Prof. Shi Zhang Qiao's group at The University of Adelaide from 2014 to 2019 as a postdoctoral researcher. Currently, he is a full professor at Huazhong University of Science and Technology. His research focuses on integration-designed electro-activation (IDEA) for renewable energy.

■ ACKNOWLEDGMENTS

This work was supported by The National Key Research and Development Program of China (2021YFA1600800), the Start-up Funding of the Huazhong University of Science and Technology (HUST), the Program for HUST Academic Frontier Youth Team, The Innovation and Talent Recruitment Base of New Energy Chemistry and Device (B21003), the US National Science Foundation (CHE-1914546 and CHE-2102220), and the Herman Frasch Foundation (820-HF17).

■ REFERENCES

(1) Jiang, N.; You, B.; Sheng, M.; Sun, Y. Electrodeposited Cobalt-Phosphorous-Derived Films as Competent Bifunctional Catalysts for Overall Water Splitting. *Angew. Chem., Int. Ed.* **2015**, *54*, 6251−6254.

(2) You, B.; Liu, X.; Hu, G.; Gul, S.; Yano, J.; Jiang, D. E.; Sun, Y. Universal Surface Engineering of Transition Metals for Superior Electrocatalytic Hydrogen Evolution in Neutral Water. *J. Am. Chem. Soc.* **2017**, *139*, 12283−12290.

(3) Zhao, H.; Lu, D.; Wang, J.; Tu, W.; Wu, D.; Koh, S. W.; Gao, P.; Xu, Z. J.; Deng, S.; Zhou, Y.; You, B.; Li, H. Raw Biomass Electroreforming Coupled to Green Hydrogen Generation. *Nat. Commun.* **2021**, *12*, 2008.

(4) Du, L.; Xiong, H.; Lu, H.; Yang, L.-M.; Liao, R.-Z.; Xia, B. Y.; You, B. Electroshock Synthesis of a Bifunctional Nonprecious Multi-Element Alloy for Alkaline Hydrogen Oxidation and Evolution. *Exploration* **2022**, *2*, 20220024.

(5) Kumar, A.; Daw, P.; Milstein, D. Homogeneous Catalysis for Sustainable Energy: Hydrogen and Methanol Economies, Fuels from Biomass, and Related Topics. *Chem. Rev.* **2022**, *122*, 385−441.

(6) Wang, C.; Astruc, D. Recent Developments of Nanocatalyzed Liquid-Phase Hydrogen Generation. *Chem. Soc. Rev.* **2021**, *50*, 3437−3484.

(7) Kammen, D. M.; Lipman, T. E. Assessing the Future Hydrogen Economy. *Science* **2003**, *302*, 226−229.

(8) Yang, Y.; Peltier, C. R.; Zeng, R.; Schimmenti, R.; Li, Q.; Huang, X.; Yan, Z.; Potsi, G.; Selhorst, R.; Lu, X.; Xu, W.; Tader, M.; Soudackov, A. V.; Zhang, H.; Krumov, M.; Murray, E.; Xu, P.; Hitt, J.; Xu, L.; Ko, H. Y.; Ernst, B. G.; Bundschu, C.; Luo, A.; Markovich, D.; Hu, M.; He, C.; Wang, H.; Fang, J.; DiStasio, R. A., Jr; Kourkoutis, L. F.; Singer, A.; Noonan, K. J. T.; Xiao, L.; Zhuang, L.; Pivovar, B. S.; Zelenay, P.; Herrero, E.; Feliu, J. M.; Suntivich, J.; Giannelis, E. P.; Hammes-Schiffer, S.; Arias, T.; Mavrikakis, M.; Mallouk, T. E.; Brock, J. D.; Muller, D. A.; DiSalvo, F. J.; Coates, G. W.; Abruna, H. D. Electrocatalysis in Alkaline Media and Alkaline Membrane-Based Energy Technologies. *Chem. Rev.* **2022**, *122*, 6117−6321.

(9) Zhao, X.; He, D.; Xia, B. Y.; Sun, Y.; You, B. Ambient Electrosynthesis toward Single-Atom Sites for Electrocatalytic Green Hydrogen Cycling. *Adv. Mater.* **2023**, *35*, 2210703.

(10) Li, X.; Lei, H.; Xie, L.; Wang, N.; Zhang, W.; Cao, R. Metalloporphyrins as Catalytic Models for Studying Hydrogen and Oxygen Evolution and Oxygen Reduction Reactions. *Acc. Chem. Res.* **2022**, *55*, 878−892.

(11) Wu, L.; Li, Y.; Fu, Z.; Su, B. L. Hierarchically Structured Porous Materials: Synthesis Strategies and Applications in Energy Storage. *Natl. Sci. Rev.* **2020**, *7*, 1667−1701.

(12) Cai, G.; Yan, P.; Zhang, L.; Zhou, H. C.; Jiang, H.-L. Metal-Organic Framework-Based Hierarchically Porous Materials: Synthesis and Applications. *Chem. Rev.* **2021**, *121*, 12278−12326.

(13) Hara, Y.; Kanamori, K.; Nakanishi, K. Self-Assembly of Metal-Organic Frameworks into Monolithic Materials with Highly Controlled Trimodal Pore Structures. *Angew. Chem., Int. Ed.* **2019**, *58*, 19047−19053.

(14) Peng, M.; Shi, D.; Sun, Y.; Cheng, J.; Zhao, B.; Xie, Y.; Zhang, J.; Guo, W.; Jia, Z.; Liang, Z.; Jiang, L. 3D Printed Mechanically Robust Graphene/CNT Electrodes for Highly Efficient Overall Water Splitting. *Adv. Mater.* **2020**, *32*, 1908201.

(15) Li, R.; Liu, X.; Wu, R.; Wang, J.; Li, Z.; Chan, K. C.; Wang, H.; Wu, Y.; Lu, Z. Flexible Honeycombed Nanoporous/Glassy Hybrid for Efficient Electrocatalytic Hydrogen Generation. *Adv. Mater.* **2019**, *31*, 1904989.

(16) Zhang, Y.; Wu, M.; Zhu, Q.; Wang, F.; Su, H.; Li, H.; Diao, C.; Zheng, H.; Wu, Y.; Wang, Z. L. Performance Enhancement of Flexible Piezoelectric Nanogenerator via Doping and Rational 3D Structure Design For Self-Powered Mechanosensational System. *Adv. Funct. Mater.* **2019**, *29*, 1904259.

(17) Chen, Q.; Wiedenroth, H. S.; German, S. R.; White, H. S. Electrochemical Nucleation of Stable N_2 Nanobubbles at Pt Nanoelectrodes. *J. Am. Chem. Soc.* **2015**, *137*, 12064−12069.

(18) German, S. R.; Edwards, M. A.; Ren, H.; White, H. S. Critical Nuclei Size, Rate, and Activation Energy of H_2 Gas Nucleation. *J. Am. Chem. Soc.* **2018**, *140*, 4047−4053.

(19) Shin, H. C.; Dong, J.; Liu, M. Nanoporous Structures Prepared by an Electrochemical Deposition Process. *Adv. Mater.* **2003**, *15*, 1610−1614.

(20) Tsai, W.; Hsu, P.; Hwu, Y.; Chen, C.; Chang, L.; Je, J.; Lin, H.; Groso, A.; Margaritondo, G. Building on Bubbles in Metal Electrodeposition. *Nature* **2002**, *417*, 139.

(21) Shin, H.-C.; Liu, M. Copper Foam Structures with Highly Porous Nanostructured Walls. *Chem. Mater.* **2004**, *16*, 5460−5464.

(22) Li, H.; Han, X.; Zhao, W.; Azhar, A.; Jeong, S.; Jeong, D.; Na, J.; Wang, S.; Yu, J.; Yamauchi, Y. Electrochemical Preparation of Nano/Micron Structure Transition Metal-Based Catalysts for the Oxygen Evolution Reaction. *Mater. Horiz.* **2022**, *9*, 1788−1824.

(23) Nørskov, J. K.; Bligaard, T.; Logadottir, A.; Kitchin, J. R.; Chen, J. G.; Pandelov, S.; Stimming, U. Trends in the Exchange Current for Hydrogen Evolution. *J. Electrochem. Soc.* **2005**, *152*, J23−J26.
(24) Nikolić, N. D.; Popov, K. I.; Pavlović, L. J.; Pavlović, M. G. The Effect of Hydrogen Codeposition on the Morphology of Copper Electrodeposits. I. The Concept of Effective Overpotential. *J. Electroanal. Chem.* **2006**, *588*, 88−98.
(25) Plowman, B. J.; Jones, L. A.; Bhargava, S. K. Building with Bubbles: the Formation of High Surface Area Honeycomb-like Films via Hydrogen Bubble Templated Electrodeposition. *Chem. Commun.* **2015**, *51*, 4331−4346.
(26) Nam, D.; Kim, R.; Han, D.; Kim, J.; Kwon, H. Effects of $(NH_4)_2SO_4$ and BTA on the Nanostructure of Copper foam Prepared by Electrodeposition. *Electrochim. Acta* **2011**, *56*, 9397−9405.
(27) Sun, Y.; Liu, C.; Grauer, D. C.; Yano, J.; Long, J. R.; Yang, P.; Chang, C. J. Electrodeposited Cobalt-Sulfide Catalyst for Electrochemical and Photoelectrochemical Hydrogen Generation from Water. *J. Am. Chem. Soc.* **2013**, *135*, 17699−17702.
(28) Jiang, N.; Bogoev, L.; Popova, M.; Gul, S.; Yano, J.; Sun, Y. Electrodeposited Nickel-Sulfide Films as Competent Hydrogen Evolution Catalysts in Neutral Water. *J. Mater. Chem. A* **2014**, *2*, 19407−19414.
(29) Jiang, N.; You, B.; Boonstra, R.; Terrero Rodriguez, I. M.; Sun, Y. Integrating Electrocatalytic 5-Hydroxymethylfurfural Oxidation and Hydrogen Production via Co-P-Derived Electrocatalysts. *ACS Energy Lett.* **2016**, *1*, 386−390.
(30) Jiang, N.; You, B.; Sheng, M.; Sun, Y. Bifunctionality and Mechanism of Electrodeposited Nickel-Phosphorous Films for Efficient Overall Water Splitting. *ChemCatChem.* **2016**, *8*, 106−112.
(31) You, B.; Liu, X.; Liu, X.; Sun, Y. Efficient H_2 Evolution Coupled with Oxidative Refining of Alcohols via A Hierarchically Porous Nickel Bifunctional Electrocatalyst. *ACS Catal.* **2017**, *7*, 4564−4570.
(32) Li, G.; Han, G.; Wang, L.; Cui, X.; Moehring, N. K.; Kidambi, P. R.; Jiang, D. E.; Sun, Y. Dual Hydrogen Production from Electrocatalytic Water Reduction Coupled with Formaldehyde Oxidation via a Copper-Silver Electrocatalyst. *Nat. Commun.* **2023**, *14*, 525.
(33) You, B.; Jiang, N.; Sheng, M.; Bhushan, M. W.; Sun, Y. Hierarchically Porous Urchin-Like Ni_2P Superstructures Supported on Nickel Foam as Efficient Bifunctional Electrocatalysts for Overall Water Splitting. *ACS Catal.* **2016**, *6*, 714−721.
(34) You, B.; Sun, Y. Hierarchically Porous Nickel Sulfide Multifunctional Superstructures. *Adv. Energy Mater.* **2016**, *6*, 1502333.
(35) Song, F.; Li, W.; Yang, J.; Han, G.; Liao, P.; Sun, Y. Interfacing Nickel Nitride and Nickel Boosts Both Electrocatalytic Hydrogen Evolution and Oxidation Reactions. *Nat. Commun.* **2018**, *9*, 4531.
(36) Song, F.; Li, W.; Yang, J.; Han, G.; Yan, T.; Liu, X.; Rao, Y.; Liao, P.; Cao, Z.; Sun, Y. Interfacial Sites between Cobalt Nitride and Cobalt Act as Bifunctional Catalysts for Hydrogen Electrochemistry. *ACS Energy Lett.* **2019**, *4*, 1594−1601.
(37) Nikolić, N. D.; Branković, G.; Maksimović, V. M.; Pavlović, M. G.; Popov, K. I. Application of Pulsating Overpotential Regime on the Formation of Copper Deposits in the Range of Hydrogen Codeposition. *J. Solid State Electrochem.* **2010**, *14*, 331−338.
(38) Ghaemi, M.; Binder, L. Effects of Direct and Pulse Current on Electrodeposition of Manganese Dioxide. *J. Power Sources* **2002**, *111*, 248−254.
(39) Yao, R. Q.; Zhou, Y. T.; Shi, H.; Wan, W. B.; Zhang, Q. H.; Gu, L.; Zhu, Y. F.; Wen, Z.; Lang, X. Y.; Jiang, Q. Nanoporous Surface High-Entropy Alloys as Highly Efficient Multisite Electrocatalysts for Nonacidic Hydrogen Evolution Reaction. *Adv. Funct. Mater.* **2021**, *31*, 2009613.
(40) Huang, J.; Han, J.; Wu, T.; Feng, K.; Yao, T.; Wang, X.; Liu, S.; Zhong, J.; Zhang, Z.; Zhang, Y.; Song, B. Boosting Hydrogen Transfer during Volmer Reaction at Oxides/Metal Nanocomposites for Efficient Alkaline Hydrogen Evolution. *ACS Energy Lett.* **2019**, *4*, 3002−3010.
(41) Chen, G.; Xu, C.; Huang, X.; Ye, J.; Gu, L.; Li, G.; Tang, Z.; Wu, B.; Yang, H.; Zhao, Z.; Zhou, Z.; Fu, G.; Zheng, N. Interfacial Electronic Effects Control The Reaction Selectivity of Platinum Catalysts. *Nat. Mater.* **2016**, *15*, 564−569.
(42) Li, Z.; Cui, Y.; Wu, Z.; Milligan, C.; Zhou, L.; Mitchell, G.; Xu, B.; Shi, E.; Miller, J. T.; Ribeiro, F. H.; Wu, Y. Reactive Metal-Support Interactions at Moderate Temperature in Two-Dimensional Niobium-Carbide-Supported Platinum Catalysts. *Nat. Catal.* **2018**, *1*, 349−355.
(43) You, B.; Zhang, Y.; Jiao, Y.; Davey, K.; Qiao, S. Z. Negative Charging of Transition-Metal Phosphides via Strong Electronic Coupling for Destabilization of Alkaline Water. *Angew. Chem., Int. Ed.* **2019**, *58*, 11796−11800.
(44) You, B.; Jiang, N.; Sheng, M.; Gul, S.; Yano, J.; Sun, Y. High-Performance Overall Water Splitting Electrocatalysts Derived from Cobalt-Based Metal-Organic Frameworks. *Chem. Mater.* **2015**, *27*, 7636−7642.
(45) Liu, X.; You, B.; Sun, Y. Facile Surface Modification of Ubiquitous Stainless Steel Led to Competent Electrocatalysts for Overall Water Splitting. *ACS Sustain. Chem. Eng.* **2017**, *5*, 4778−4784.
(46) You, B.; Jiang, N.; Liu, X.; Sun, Y. Simultaneous H_2 Generation and Biomass Upgrading in Water by an Efficient Noble-Metal-Free Bifunctional Electrocatalyst. *Angew. Chem. Int., Ed.* **2016**, *55*, 9913−9917.
(47) You, B.; Liu, X.; Jiang, N.; Sun, Y. A General Strategy for Decoupled Hydrogen Production from Water Splitting by Integrating Oxidative Biomass Valorization. *J. Am. Chem. Soc.* **2016**, *138*, 13639−13646.
(48) You, B.; Sun, Y. Innovative Strategies for Electrocatalytic Water Splitting. *Acc. Chem. Res.* **2018**, *51*, 1571−1580.
(49) Zhuang, Z.; Giles, S. A.; Zheng, J.; Jenness, G. R.; Caratzoulas, S.; Vlachos, D. G.; Yan, Y. Nickel Supported on Nitrogen-Doped Carbon Nanotubes as Hydrogen Oxidation Reaction Catalyst in Alkaline Electrolyte. *Nat. Commun.* **2016**, *7*, 10141.
(50) Chen, Q.; Luo, L.; Faraji, H.; Feldberg, S. W.; White, H. S. Electrochemical Measurements of Single H_2 Nanobubble Nucleation and Stability at Pt Nanoelectrodes. *J. Phys. Chem. Lett.* **2014**, *5*, 3539−3544.
(51) Hall, A. S.; Yoon, Y.; Wuttig, A.; Surendranath, Y. Mesostructure-Induced Selectivity in CO_2 Reduction Catalysis. *J. Am. Chem. Soc.* **2015**, *137*, 14834−14837.
(52) Yoon, Y.; Hall, A. J.; Surendranath, Y. Tuning of Silver Catalyst Mesostructure Promotes Selective Carbon Dioxide Conversion into Fuels. *Angew. Chem. Int., Ed.* **2016**, *55*, 15282−15286.
(53) You, B.; Jiang, N.; Sheng, M.; Drisdell, W. S.; Yano, J.; Sun, Y. Bimetal-Organic Framework Self-Adjusted Synthesis of Support-Free Nonprecious Electrocatalysts for Efficient Oxygen Reduction. *ACS Catal.* **2015**, *5*, 7068−7076.
(54) Tian, X.; Lu, X. F.; Xia, B. Y.; Lou, X. W. Advanced Electrocatalysts for the Oxygen Reduction Reaction in Energy Conversion Technologies. *Joule* **2020**, *4*, 45−68.

https://doi.org/10.1021/acs.accounts.3c00059
Acc. Chem. Res. 2023, 56, 1421−1432